Comparative study of Ergosterol and 7-dehydrocholesterol and their Endoperoxides: Generation, Identification and Impact in Phospholipid Membranes and Melanoma Cells

Megumi Nishitani Yukuyama [a,*, **], Karen Campos Fabiano [a,*], Alex Inague [#], Miriam Uemi [b], Rodrigo Santiago Lima [a], Larissa Regina Diniz [a], Tiago Eugenio Oliveira [a], Thais Satie Iijima [a], Hector Oreliana Fernandes Faria [a], Rosangela Silva Santos [a], Maria Fernanda Valente Nolf [a], Adriano Brito Chaves-Filho [##], Marcos Yukio Yoshinaga [a], Helena Couto Junqueira [a], Paolo Di Mascio [a], Mauricio da Silva Baptista [a], Sayuri Miyamoto [a,**]

* Equivalent authors

** Corresponding authors:
miyamoto@iq.usp.br; Av. Prof. Lineu Prestes, 748 - Butantan, São Paulo - SP, 05508-900, Brazil
meguminishitani@hotmail.com; Av. Prof. Lineu Prestes, 748 - Butantan, São Paulo - SP, 05508-900, Brazil

a *Department of Biochemistry, Institute of Chemistry, University of Sao Paulo, Av. Prof Lineu Prestes 1524, São Paulo 05508000, Brazil*
b Institute of Environmental, Chemical and Pharmaceutical Sciences, Federal University of São Paulo, Rua São Nicolau, 210, Centro, Diadema, São Paulo 09913-030, Brazil
 # Department of Nutritional Sciences and Toxicology, University of California, Berkeley, Berkeley, CA, USA; Li Ka Shing Center for Biomedical Sciences, 1951 Oxford Street, UC Berkeley 94720
Division of Tumor Metabolism and Microenvironment, German Cancer Research Center (DKFZ), Im Neuenheimer Feld 581, 69120 Heidelberg, Germany

Keywords: ergosterol, 7-dehydrocholesterol, endoperoxide, photooxidation, singlet oxygen, melanoma, photodynamic therapy

ABSTRACT

Melanoma is an aggressive cancer that has attracted attention in recent years due to its high mortality rate of 80%. Damage caused by oxidative stress generated by radical oxidation (type I reaction) and singlet oxygen (type II reaction) oxidative reactions may induce cancer. Thus, studies that aim to unveil the mechanism that drives these oxidative damage processes become relevant. Ergosterol, an analogue of 7-dehydrocholesterol (7-DHC), important in the structure of cell membranes, is widely explored in cancer treatment. However, to date little is known about the impact of different oxidative reactions on these sterols in melanoma treatment, and conflicting results about their effectiveness complicates the understanding of their role in oxidative damage. Our results highlight differences among ergosterol, 7-DHC and cholesterol in membrane properties when subjected to distinct oxidative reactions. Furthermore, we conducted a comparative study exploring mechanisms of cell damage by photodynamic treatment in A375 melanoma, comparing ergosterol, 7-DHC, and their respective endoperoxides. Notably, endoperoxides generated by singlet oxygen showed superior efficacy in reducing the viability of A375 cells compared to their precursor molecules. We also describe a step-by-step process to produce and identify endoperoxides derived from ergosterol and 7-DHC. While further studies are needed, this work provides new insights for understanding cancer cell death induced by different oxidative reactions in the presence of biologically relevant sterols.

INTRODUCTION

Skin cancer was reported to be the fifth most common cancer worldwide in 2020. It is divided in non-melanoma (basal cell carcinoma and squamous cell carcinoma) and melanoma. Although melanoma corresponds to only 4% of total skin cancer, it is considered the most dangerous due to its high death rate of 80% (1). A total of 325,000 new cases of melanoma and 57,000 deaths were estimated for 2020 worldwide, and an increase of approximately 50% of new cases and 68% deaths are projected for 2040 (2).

62 Thus, a convenient treatment becomes crucial for the improvement of the survival rate of
63 this disease.

64 Sunlight exerts many beneficial effects such as vitamin D synthesis, anti-
65 inflammatory stimulation, and prevention against several diseases (e.g., certain types of
66 cancers, diabetes, and multiple sclerosis) (3). However, excess radiation may lead to
67 negative effects causing oxidative stress and inflammation to skin cells: both UV and
68 visible light have the potential to promote photoexcitation of endogenous
69 photosensitizers, which can convert light energy into chemical energy and produce
70 reactive oxygen species (ROS), leading to redox imbalance in the cells under excessive
71 radiation (4). Examples of endogenous photosensitizers are porphyrins, flavin, melanin,
72 and lipofuscin, and the concentration and presence of these photosensitizers influence
73 the sensitivity of specific tissue or cells to photoinduced damage (5). Photooxidation
74 reactions are classified as Type I or Type II reactions. Type I reaction generates reactive
75 radical species, such as superoxide radical anion ($O_2^{\bullet-}$) and hydroperoxyl radicals
76 ($HOO^{\bullet}$), while type II reactions generate singlet molecular oxygen ($^1O_2$) (6). Although
77 current photoprotection products block UV rays, emerging studies show that
78 photodamage by visible light is responsible for more than 50% of skin radicals generated
79 under sun exposure (4, 7) . Among several biomolecules, lipids play essential roles in cell
80 membrane structure, serve as energy source, and generate metabolites that support
81 proper cell development and proliferation (8) Lipids are classified into various categories,
82 including glycerolipids, and sterol lipids. Cholesterol is essential for cell membrane
83 structure and as a precursor for other steroidal biomolecules such as hormones and
84 vitamin D (9, 10). When oxidized, cholesterol gives rise to oxidized derivatives, known as
85 oxysterols, including reactive sterol electrophiles that may disturb cellular function,
86 leading to several diseases including cancer (11).

87 Ergosterol (Erg) was first discovered in 1889 in extracts of the ergot fungus
88 (*Claviceps purpurea*) by Tanret and described as the major sterol of fungi (12). This sterol
89 is found mainly in the lipid bilayer of the cell membranes of most fungi and is essential for
90 cell maintenance and growth (13). Erg has a similar function and structure to cholesterol,
91 differing by two additional double bonds at the C_7 and C_{22} positions and a methyl bond at
92 the C_{24} position (**Figure 1**). Increasing attention has been given to Erg and its derivatives

93 given their properties to inhibit cell growth efficacy in several cancer cells, by interacting
94 with JAK/STAT mechanism or caspase-independent apoptos (14, 15). Additionally,
95 studies have indicated that oxidized derivatives of Erg, such as the 5α, 8α-
96 epidioxiergosta-6, 22-dien-3β-ol (EEP), an Erg peroxide purified from *Ganoderma*
97 *lucidum*, induce human hepatocellular carcinoma cell death through the activation of pro-
98 apoptotic protein Puma and Bax under stimulation of Foxo3 activity by EEP (16).

99 7-dehydrocholesterol (7-DHC) is a precursor of cholesterol in mammals, with a
100 very similar structure to Erg (**Figure 1**) (17, 18) . The anticancer effect of 7-DHC in the
101 melanoma A2058 cell line was demonstrated by the dose-dependent decrease in its
102 viability. In the absence of light, cells treated with 7-DHC generated ROS, increased pro-
103 apoptotic Bax protein, and affected mitochondrial permeabilization by reducing
104 mitochondria membrane potential (19). Additionally, in ovarian cancer, replacing
105 cholesterol with 7-DHC significantly enhanced the anticancer activity of photosensitizer-
106 encapsulated liposomes upon irradiation (20). In contrast, other studies demonstrated
107 that 7-DHC suppressed and regulated cell death by ferroptosis, an iron-dependent non-
108 apoptotic cell death caused by exacerbated lipid peroxidation (21, 22). It has been shown
109 that pre-treatment of B16F10 melanoma cells with 7-DHC significantly protected cells
110 from ferroptosis, suggesting that 7-DHC can increase melanoma resistance against
111 oxidative stress (21).

112 Given conflicting results mentioned above and considering the cell death caused
113 by lipid oxidation reactions, we were interested in comparing the damage to the cell
114 membrane caused by sterols under oxidation reactions type I and type II. It was also our
115 interest to compare the cancer cell death efficacy of these products and their respective
116 endoperoxides. Thus, this work aims to present a step-by-step process to produce
117 endoperoxide derivatives of Erg and 7-DHC and determine whether they protected lipid
118 bilayers against Type I or Type II photooxidative damage and their influence on
119 melanoma A375 cell viability.

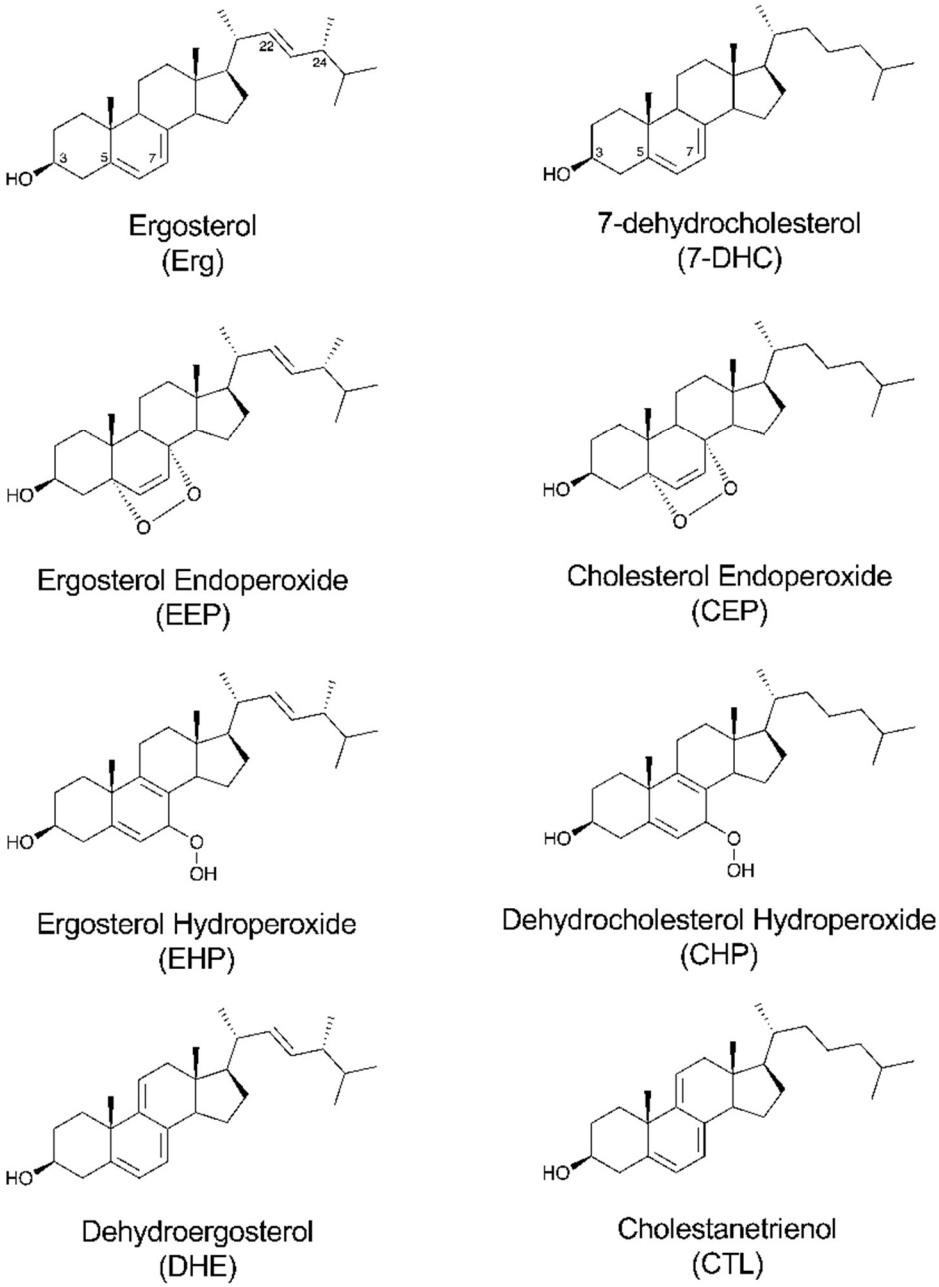

Figure 1. Structure of 7-dehidrocholesterol and ergosterol and their oxidation products.

MATERIALS

Phospholipids palmitoyl-oleoyl phosphatidylcholine (POPC, 1-palmitoyl-2-oleoyl-sn-glycero-3-phosphocholine) and egg yolk phosphatidylcholine (EggPC, L-α-phosphatidylcholine) were purchased from Avanti Polar Lipids (Alabaster, USA). Solvents (HPLC grade) were purchased from Merck (Darmstadt, Germany), methylene blue,

128 DMMB and other reagents were purchased from Sigma-Aldrich (St. Louis, USA). Fetal
129 bovine serum, penicillin-streptomycin and DMEM, high glucose, GlutaMAX Supplement,
130 and pyruvate were purchased from Gibco (ThermoFischer Scientific). Deuterium
131 chloroform ($CDCl_3$) was purchased from Sigma Aldrich (Steinheim, Germany)

132

133 **METHODS**

134

135 **Synthesis and purification of sterol oxidation products**

136

137 *Sterol photo-oxidation*

138 First, 200 mg of sterol (Erg, 7-DHC or cholesterol) were dissolved in 40 mL of
139 chloroform in a 100 mL round-bottom flask, and 50 µL of the photosensitizer methylene
140 blue (10 mM in methanol) was added. This solution was placed in an ice bath and an
141 aliquot was collected at time zero. The mixture of sterol and methylene blue was kept
142 under oxygen flow and stirred under a 500 W tungsten lamp for 90 minutes (Erg and 7-
143 DHC) or 5 hours (cholesterol). Aliquots were collected in every 30 minutes for qualitative
144 analysis by thin layer chromatography (TLC) using a silica plate eluted with ethyl acetate
145 and isooctane (1:1 v/v). Plates were air-dried, sprayed with 50% sulfuric acid, and heated
146 to allow visualization of sterols and their oxidized products. (**Figure S1).**

147

148 *Purification of sterol oxidation products*

149 Sterol photooxidation products were initially separated by flash column
150 chromatography containing silica gel in hexane. After equilibrating the column with
151 hexane, a gradient of hexane and ethyl acetate in different volume ratios, 95:5 (50 mL),
152 90:10 (50 ml), 80:20 (100 ml), 70:30 (100 ml), 60:40 (100 mL), 50:50 (50 ml) and 40:60
153 (50 ml) was used for elution. Fractions of approximately 10 mL were collected and
154 checked by TLC (**Figure S2**). Sterol oxidized products were further purified by semi-
155 preparative HPLC (LC 20AD, Prominence, Shimadzu, Kyoto, Japan) coupled to a Diode
156 Array Detector (DAD, SPDM20A, Prominence, Shimadzu, Kyoto, Japan) using the

157 following conditions: Luna C18 column (250 x 10 mm, 5 µm, 100 Å); flow rate 5 mL/min;
158 40°C and mobile phase consisted of 95% Methanol and 5% water. Each peak was
159 collected in an amber glass tube using a fraction collector ((FRC10-A, Shimadzu, Kyoto,
160 Japan) and dried with the rotary evaporator.
161
162 **Characterization of sterol photooxidation products**
163
164 *Analysis of oxidation products by HPLC-DAD*
165 Sterol oxidation products were analyzed by HPLC (Prominence, Shimadzu, Kyoto,
166 Japan) coupled to a diode array detector (DAD) using a Gemini C18 column (250 x 4.6
167 mm; 5 µm, 110 Å), in isocratic elution at a flow rate of 1 mL/min with a mixture of 95 %
168 methanol and 5% water as mobile phase.
169
170 *Analysis of oxidation products by mass spectrometry*
171 The analysis of oxidation products was also performed via ultra-high-performance
172 liquid-chromatography (UHPLC Nexera, Shimadzu, Kyoto, Japan) coupled to an
173 electrospray ionization time-of-flight mass spectrometry (ESI-TOF-MS, Triple-TOF®
174 6600, Sciex, Concord, USA). Samples were separated on a C18 column (Acquity BEH
175 100 x 2.1; 1.7 µm, Waters) using a mobile phase composed of (A) water with 0.1% formic
176 acid and (B) acetonitrile with 0.1% formic acid. The following solvent gradient was used
177 for sterol oxidation analysis: 50 to 100 %B in 4.5 min, 100 % from 4.5-8.5 min, 100 to 50
178 % B from 8.5-9.0 min, and 50% B from 9-13 min. MS data were acquired in positive
179 ionization mode. All data were obtained in data-dependent acquisition mode (IDA®,
180 Information Dependent analysis) using Analyst® 1.7.1 software.
181 Sterols and their photo-oxidation products were diluted in isopropanol and
182 centrifuged at 1500 rpm for 5 minutes before injection. The following precursor ions were
183 selected for MS/MS analysis: m/z 411 (ergosterol hydroperoxide, EHP), m/z 429 (5α,8α-
184 epidioxy-22*E*-ergosta-6,9(11),22-trien-3β-ol, EEP), m/z 377 ((22E)ergosta-5,7,9,22-
185 tetraen-3β-ol , DHE) and m/z 380 (Erg) were monitored, and the data were processed
186 using the Peak View software.

187

188 *Identification of oxidation products by 1H-NMR:*

189 The ^{1}H NMR (500.13 MHz) spectra were recorded at 0 or 25 °C, using $CDCl_3$ as
190 solvent. The analyses were performed on a Bruker-Biospin Ascend 500 instrument,
191 Avance III series, (Rheinstetten, Germany), operating at 11.7 T. The instrument was
192 equipped with 5-mm trinuclear, inverse detection probe with z-gradient (TXI) or 5mm TCI
193 CryoProbe. The temperature was controlled by a BCU I accessory. All chemical shifts
194 were expressed in ppm relative to TMS. The data were acquired and processed using
195 TOPSPIN 3.5 software (Bruker-Biospin, Rheinstetten, Germany).

196

197 *Stability test of ergosterol and endoperoxides:*

198 Sterol stock solutions and endoperoxide solutions were dried with N_2 and
199 resuspended in chloroform maintaining a concentration of 1 mM. These vials were
200 placed in a thermomixer for 5h at 37ºC under stirring at 600 rpm. The aliquots were
201 collected at times zero, 1h, 2h, 3h, 4h and 5h and analysis were carried out by HPLC-
202 DAD.

203

204

205 **Analysis of liposome membrane leakage using a carboxyfluorescein system**

206

207 *Liposome membrane leakage with 1,9-dimethyl-methylene blue (DMMB)*

208 Liposomes containing phosphatidylcholine and sterols were prepared by a method
209 adapted from Miyamoto *et al.* (2012) (23). Membranes containing 50 mM
210 carboxyfluorescein (CF) were prepared by mixing POPC (1-palmitoyl-2-oleoyl-sn-
211 glycero-3-phosphocholine) and sterols (Erg, cholesterol, and 7-DHC) in 10 mM Tris buffer
212 at pH 8. Four liposomes were prepared: one with 100% POPC as a control and three
213 others combining 75% POPC with 25% of each steroid. Solutions containing each lipid
214 mixture were placed in a PYREX® test tube, vortexed, and dried under N_2 stream. The
215 samples were then left for approximately one hour in a vacuum desiccator to ensure the

216 complete removal of solvent. Then, the samples were redissolved in 500 µL of Tris buffer
217 (10 mM, pH 8) containing carboxyfluorescein (50 mM). The resulting mixture was
218 extruded with Avanti Mini-Extruder kit (Avanti Polar Lipids, Alabaster, US) equipped with
219 a 100 nm pore membrane to produce large unilamellar vesicles (LUVs) of 100 nm size.
220 CF-loaded LUVs were subjected to a Sephadex G-50 column purification using 10
221 mM Tris with 0.3 M NaCl at pH 8 as a running buffer. The CF-loaded fraction was collected
222 in a microtube and then placed in a 96-well plate at a final concentration of approximately
223 100 µM of each liposome. 15 µM DMMB was added to each well and irradiated with a
224 633 nm LED for 90 minutes. CF externalization was monitored over time with Agilent's
225 Synergy H1 Hybrid Reader equipment, using excitation at λex = 480 nm and emission at
226 λem = 517 nm. At the end of the reaction, Triton X-100 was added to release all the CF
227 content from the liposomes, to generate the final reading intensity (24, 25).
228

229 *Liposome membrane leakage by oxidation using iron/ascorbate*

230 Liposomes containing egg yolk phosphatidylcholine (EggPC) and sterols (Erg,
231 cholesterol, and 7-DHC) were prepared in Tris-HCl buffer as described in the previous
232 section, however, the DMMB solution was replaced by Fe (III)/ascorbic acid (Fe/Asc) at
233 10 µM/100 µM final concentrations. All wells contained the final concentrations of
234 approximately 100 µM of each liposome. CF release was measured as described above.
235

236 **Quantification of generated oxidized products by HPLC and Mass spectroscopy**
237

238 *Quantification of oxidation products from liposome membrane leakage test by HPLC*

239 Liposomes were produced following the same protocol described previously
240 without CF. Briefly, 200 µL of each liposome and 27 µL of DMMB 15 mM were placed in
241 a well plate and irradiated at 633 nm for 90 minutes. Then, the samples were analyzed
242 by HPLC with C8 column (Luna Phenomenex, 250 x 10 mm, 5 µm, 100 Å), isocratic mode
243 (94% MeOH and 6% water); flow rate of 1.0 mL/min at 36ºC and 30 µl sample injection
244 volume.
245

246 *Quantification of liposome phospholipids by mass spectrometry*

247 POPC was analyzed by LC/MS in the negative ionization mode, with a C18 column
248 (CORTECS Waters 2.1 mm x 10 mm; 1.6 μM) at 35 ºC. The flow rate was 0.2 mL/min;
249 injection volume was 2.0 μL, and the mobile phase was (A) water: acetonitrile (60:40); (B)
250 isopropanol: acetonitrile: water (80:10:2) with ammonium acetate (10 mM) in both phases.
251 The gradient started at 40% and increased to 100% over the first 10 minutes. It was held
252 at 100% from 10 to 12 minutes, then decreased back to 40% between 12 and 13 minutes,
253 and was maintained at 54% from 13 to 20 minutes.

254 DMPC (PC14:0/14:0) was used as an internal standard to semi-quantify POPC,
255 and its concentration was calculated by the peak area of the compound divided by the
256 peak area of the internal standard with known concentration. Aliquots of the samples (10
257 μl) were mixed with 20 μL of DMPC (5 mM) and 170 μL of isopropanol.

258

259 *Quantification of ergosterol, 7-dehydrocholesterol, and their oxidized products by mass*
260 *spectrometry:*

261 To quantify Erg, a calibration curve was built using 7-dehydrocholesterol (7-DHC)
262 as an internal standard. Working solutions for the calibration curve were prepared at
263 concentrations of Erg ranging from 15.6 μM to 1000 μM. To quantify Erg oxidation
264 products (EEP, EHP), a calibration curve was prepared with concentrations ranging from
265 0.08 μM to 20 μM, using oxidized standards prepared in the laboratory. 7-DHC
266 endoperoxide (CEP) and 7-DHC hydroperoxide (CHP) were used as internal standards
267 at final concentrations of 7.5 μM and 5 μM, respectively.

268

269 *Quantification of cholesterol and cholesterol hydroperoxides by iodometry and HPLC*

270 Cholesterol hydroperoxides (ChOOH) synthesized by photo-oxidation with
271 methylene blue were quantified by iodometry (26). The quantification of cholesterol and
272 ChOOH in the liposome after photo-oxidation with DMMB was carried out by HPLC,
273 following methods described in **Supplementary Materials**.

274

275

276 **In vitro A375 cell viability assay**

277

278 *Cell cultures*

279 A375 cells were cultured with Dulbecco's Modified Eagle's Medium-high glucose
280 (DMEM, catalog number 10569010, Thermo Fischer Scientific) supplemented with 1%
281 penicillin-streptomycin and 10% FBS. It was maintained at 37 °C under a water-saturated
282 atmosphere containing 5% CO_2, until 80%–90% confluence was reached. Cell counting
283 was performed microscopically with Trypan blue exclusion (27).

284

285 *Photodynamic treatment with sterols and DMMB*

286 Cells were incubated in a 96-well plate with increasing concentrations of sterol
287 (Erg, 7-DHC, EEP, or CEP) for 22 h. Then, DMMB (0.1 to 5 nM) (Sigma-Aldrich, São
288 Paulo, Brazil) was added and incubated for an additional 2 h. The medium was then
289 replaced with PBS, and the cell plate was irradiated at final dose of 5J/cm^2, using red light
290 with 27.84 mW/cm^2 at 660 nm λ_{max} (light source from Biolambda, Brazil).

291

292 *Cell viability assay*

293 The medium of the cell plate incubated after 0 h and 24h irradiation were discarded
294 and 0.01 g/L resazurin solution in the medium was added to each cell well. Cell viability
295 was determined by measuring fluorescence using the program SoftMax Pro 5.4.1, at 540
296 nm excitation wavelength and 590 nm emission wavelength. The viability curve was
297 prepared using GraphPad Prism 8.0.1. Data was expressed as means ± SD of at least
298 three independent experiments.

299

300

301 **RESULTS**

302

303 **Photooxidation of ergosterol and 7-dehydrocholesterol yields endoperoxides as**
304 **the most stable products**
305
306 Erg and 7-DHC were photo-oxidized in chloroform with methylene blue as a
307 photosensitizer (**Figure S1**). Aliquots of the reaction mixture were analyzed by TLC and
308 HPLC. Nearly all the sterols were consumed after 90 minutes of irradiation, resulting in
309 the formation of 3 major photo-oxidized products. Oxidized products were first purified by
310 flash column chromatography and fractions were checked by TLC (**Figure S2**). The
311 fractions containing the endoperoxide, hydroperoxide, and triene products were dried and
312 resuspended in 3 mL of isopropanol for further purification by HPLC. **Figure S3** shows
313 the peaks corresponding to the three major products that were purified by semi-
314 preparative HPLC and their estimated yields. The photooxidation of ergosterol and 7-
315 dehydrocholesterol primarily produced endoperoxides (EEP and CEP) with yields of
316 approximately 37-38%. This was followed by the formation of hydroperoxides (EHP and
317 CHP) and triene products, which were produced at lower yields.
318 After purification, each oxidation product appeared as single peaks in the HPLC
319 chromatogram, confirming their successful purification (**Figure 2**). Their identities were
320 further confirmed by high-resolution LC-MS analysis.

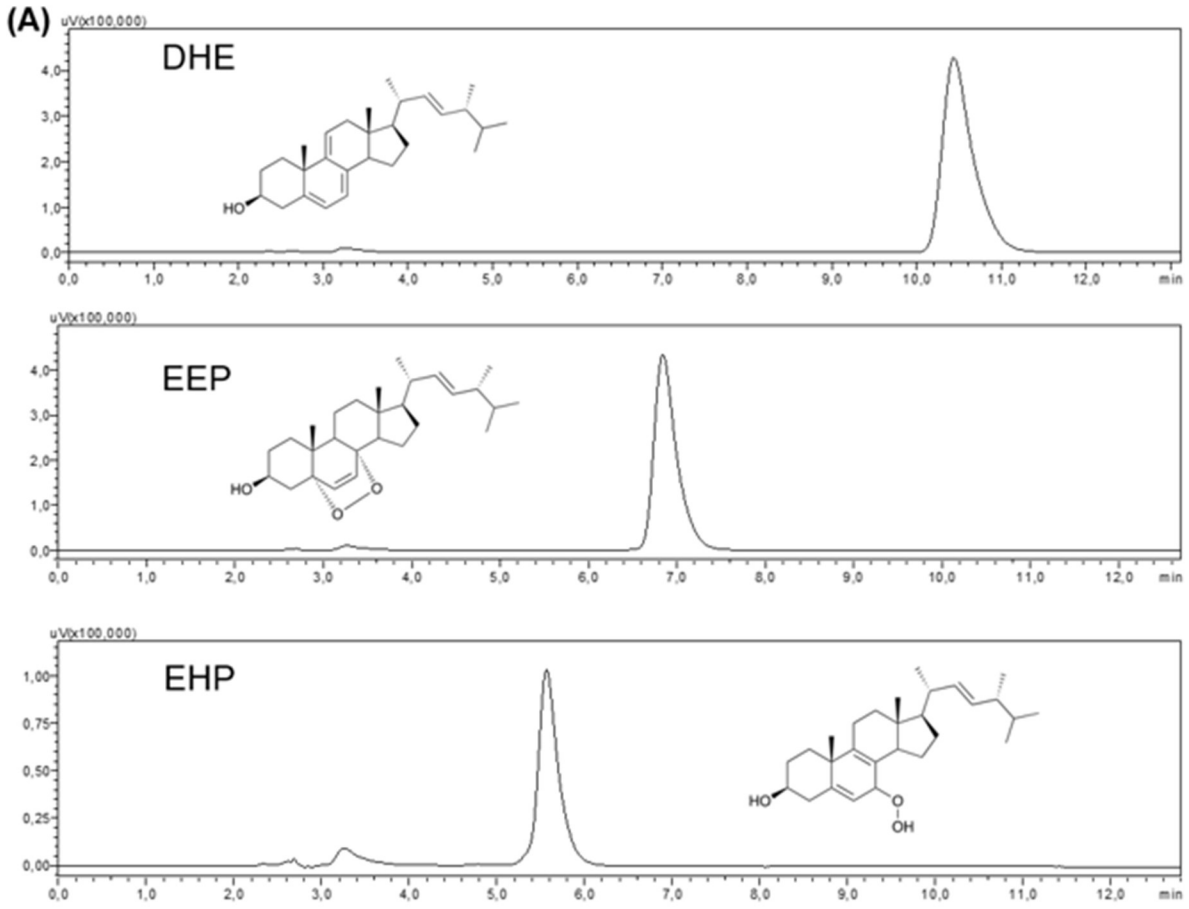

321

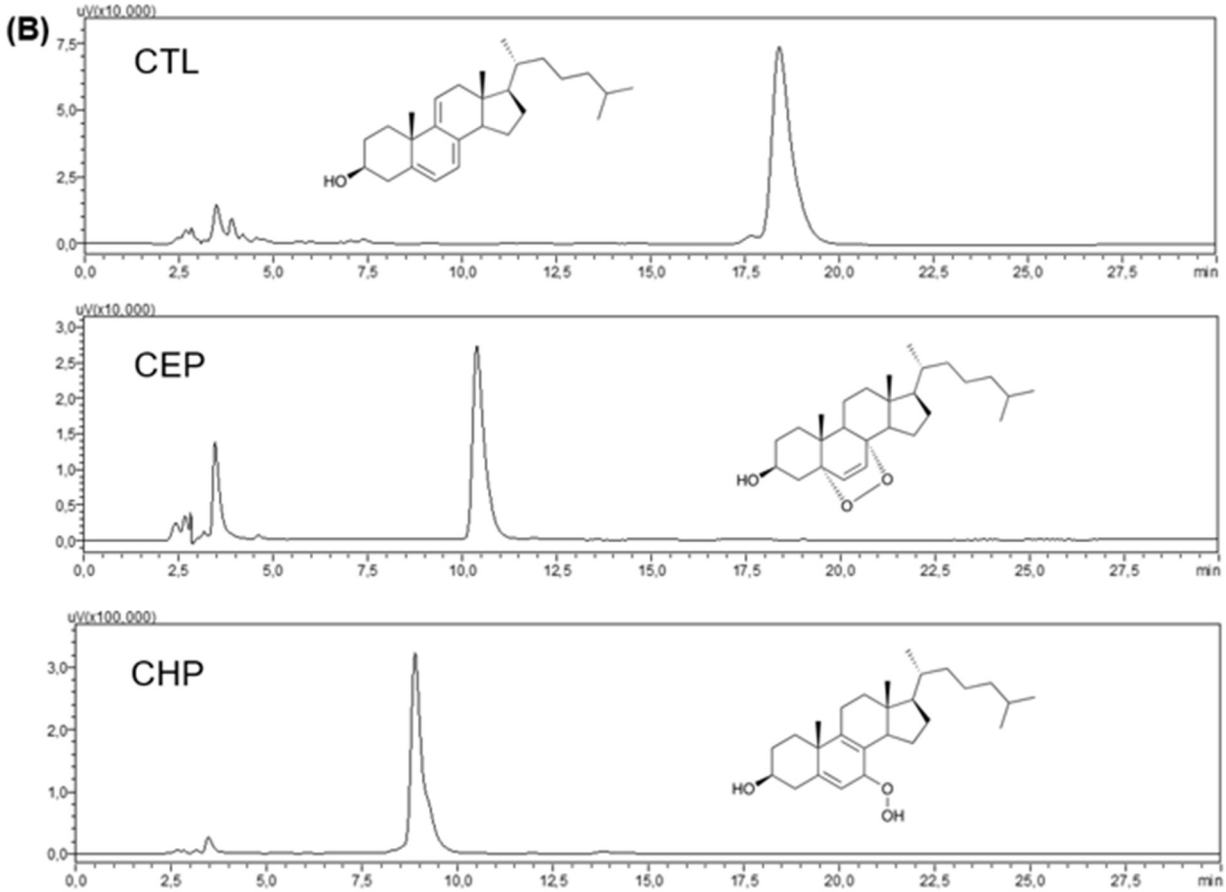

Figure 2. HPLC analysis of the purified photooxidation products derived from (A) ergosterol: dehydroergosterol (DHE), ergosterol endoperoxide (EEP), and ergosterol hydroperoxide (EHP); (B) 7-dehydrocholesterol: cholestanetrienol (CTL), 7-dehydrocholesterol endoperoxide (CEP), and 8-dehydrocholesterol hydroperoxide (CHP).

MS/MS spectra with the respective fragmentations of the purified ergosterol oxidation products are shown in **Figure 3**. EEP and DHE protonated ions $[M+H]^+$ were observed at m/z 429.3372, respectively, while for the DHE and EHP a dehydrated protonated ions $[(M-H_2O)+H]^+$ appeared as a major ion at m/z 377.3157 and 411.3257. Characteristic fragments were found at m/z 411.32, 393.31 corresponding to the loss of water and O_2 from EEP; and m/z 375.30 for EHP, corresponding to the loss of three water molecules. Endoperoxides of ergosterol and 7-DHC were further confirmed by 1H-NMR

analysis (**Figure S4**, **Table S1** and **Table S2**).

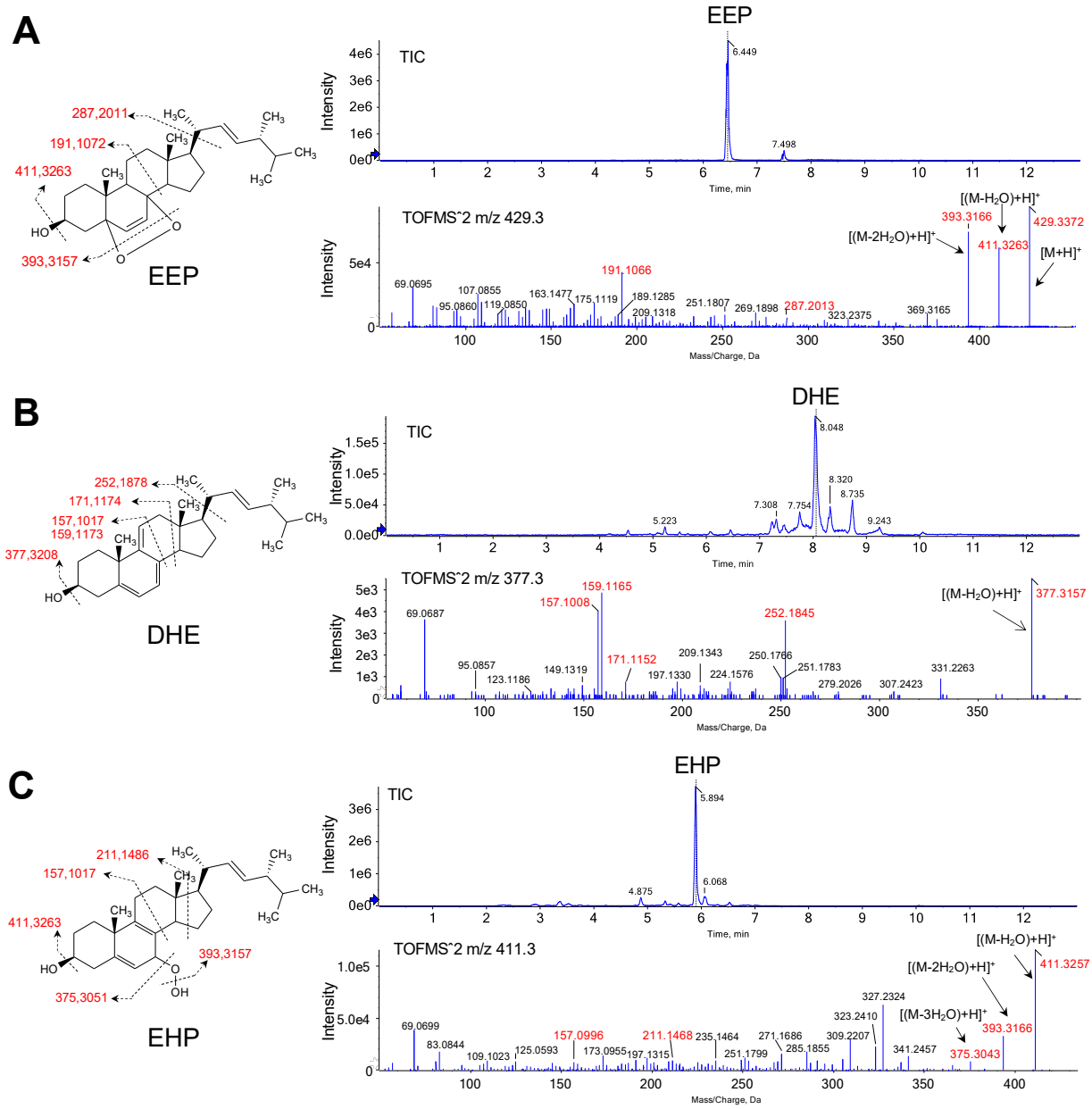

Figure 3. Extracted ion chromatogram and fragmentation spectrum obtained in MS/MS mode of Ergosterol photooxidation products: (A) EEP; (B) DHE and (C) EHP.

Next, we investigated the production of endoperoxides and hydroperoxides using dimethyl-naphthalene endoperoxide (DMNO2) as a clean source of singlet oxygen. Analysis of the oxidation products by HPLC showed that ergosterol incubation with

DMNO2 generates both EEP and EHP, suggesting that singlet oxygen reacts ergosterol double bonds through *ene* and cycloadditin reactions (**Figure 4**).

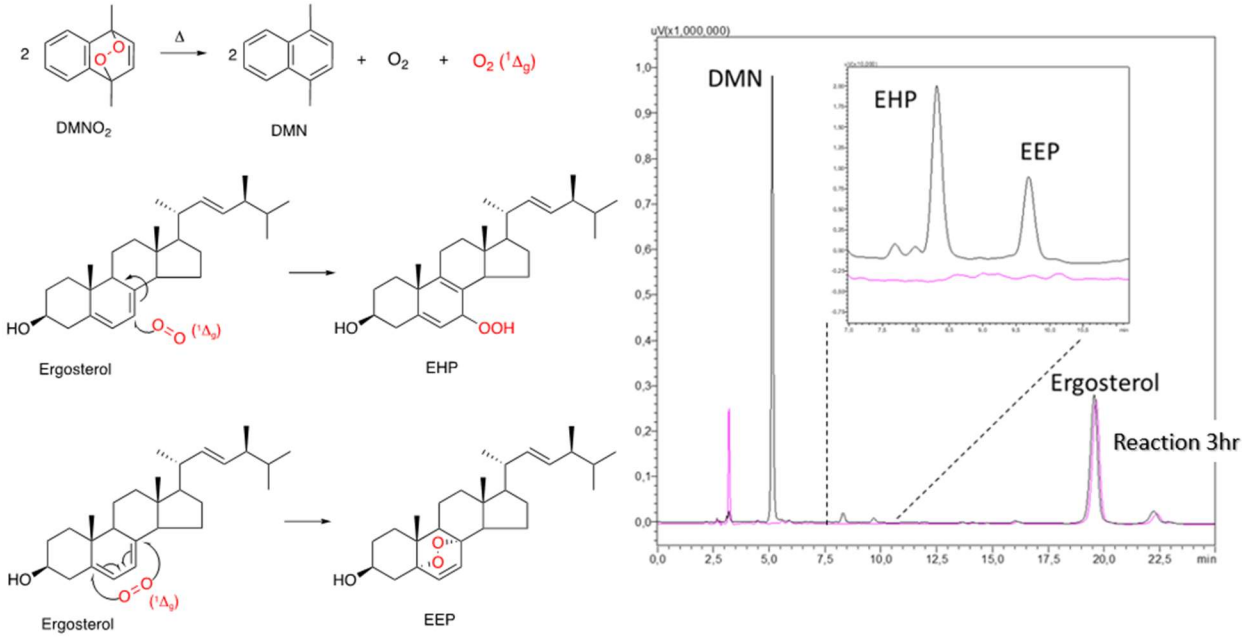

Figure 4. Chromatogram of HPLC analysis of ergosterol reaction with $DMNO_2$ monitored at 210 nm. The pink line represents the initial time and the black line the final time of the reaction.

Quantitative analysis of ergosterol oxidation products formed with increasing concentrations of DMNO2 was performed by mass spectrometry (**Figure 5**). As expected, ergosterol consumption and EEP formation increased proportionally with the generation of $^1O_2$. However, higher levels of singlet oxygen generated by DMNO2 led to a decrease in EHP levels and an increase in the formation of a third product, identified as a di-hydroperoxide (di-EHP) (**Figure S5**). These results demonstrate that the reaction of singlet oxygen with ergosterol produces EEP, EHP, and small amounts of di-hydroperoxides (**Figure 5**). Furthermore, stability analysis showed that EEP is highly stable, while EHP degrades rapidly (**Figure S6**). This suggests that EHP is formed through Type II photooxidation but is either converted to di-EHP or degraded during reaction. Overall, these findings indicate that endoperoxides is the most stable products

366 of photooxidation.

367

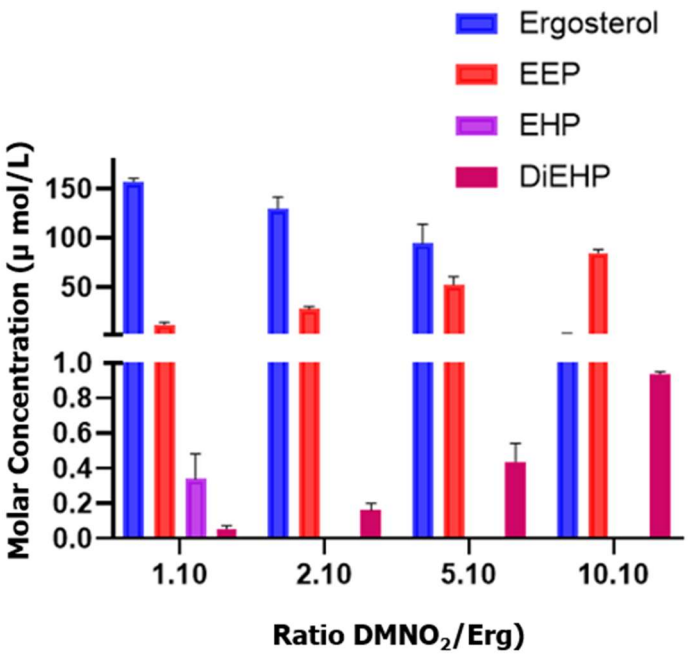

368

369 **Figure 5**. Concentration of ergosterol and products by reaction with $DMNO_2$ analyzed by

370 HPLC-MS.

371

372

373 **Sterols in liposomes exhibit distinct membrane leakage kinetics under type I and II**

374 **oxidation**

375

376 Membrane protective effects of Erg and 7-DHC were evaluated under type I and

377 type II oxidation conditions using sterol-containing liposomes loaded with

378 carboxyfluorescein. For type II oxidation (singlet oxygen), liposomes were prepared with

379 POPC (control) or POPC with 25% sterol (Erg, 7-DHC, or Cholesterol) and DMMB as a

380 photosensitizer. A significant reduction in membrane leakage was observed for liposomes

381 containing sterols (**Figure 6A**). While carboxyfluorescein release in the controls reached

382 75% after 180 minutes of irradiation, liposomes containing Erg or 7-DHC released less

383 than 35% of the probe. Notably, cholesterol provided the highest protection, with minimal

384 release of the probe (<5%). For comparison, membrane leakage studies were conducted

385 using iron/ascorbate (Fe/Asc) as a radical generator under type I oxidation. In contrast to
386 the results observed under type II oxidation, Erg and 7-DHC provided greater protection
387 to the liposome membrane than cholesterol, particularly during the initial phase of
388 oxidation propagation (**Figure 6B**), which is consistent with their high radical-trapping
389 activity.
390

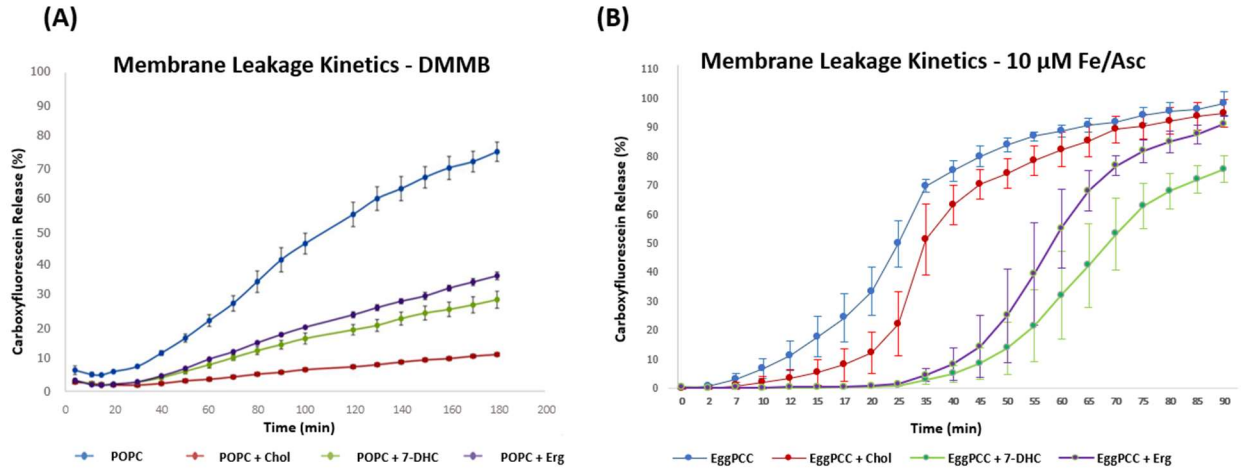

391
392

393 **Figure 6.** Leakage kinetics of carboxyfluorescein encapsulated in (A) POPC liposome in
394 the presence of the photosensitizer DMMB and (B) Egg phosphatidylcholine liposome
395 (EggPC) in the presence of 10 µM Fe/Asc. Liposomes were composed of either 100%
396 POPC or EggPC, or a mixture of 75% POPC or EggPC with 25% sterols (Erg, 7-DHC or
397 Cholesterol). Leakage was monitored by measuring fluorescence at 517 nm.
398
399

400 **Quantification of phospholipid and sterol photo-oxidation products**

401

402 *Sterols protect liposome membranes against phospholipid oxidation*

403 To investigate the membrane protective effects of Erg against photosensitized
404 oxidation, we analyzed the kinetics of phospholipid oxidation in the liposome membranes.
405 Phospholipid hydroperoxides (POPC-OOH), the primary products formed by the reaction
406 of singlet oxygen with POPC, were quantified by HPLC. As shown, the control decrease

(**Figures 7A)** was accompanied by an increase in POPC-OOH (**Figures 7B)**. In control liposomes (POPC), hydroperoxide levels reached a plateau at 20 minutes and then decreased after 40 minutes of irradiation (**Figure 7B**), likely due to the degradation of POPC-OOH forming truncated phospholipid species responsible for membrane leakage (19). In contrast, ergosterol (POPC + Erg) and cholesterol (POPC + Chol) protected membranes against phospholipid oxidation, leading to lower POPC-OOH levels compared to liposomes without sterols (POPC). Liposomes with Erg (POPC + Erg) showed the least generation of POPC-OOH (**Figure 7B**).

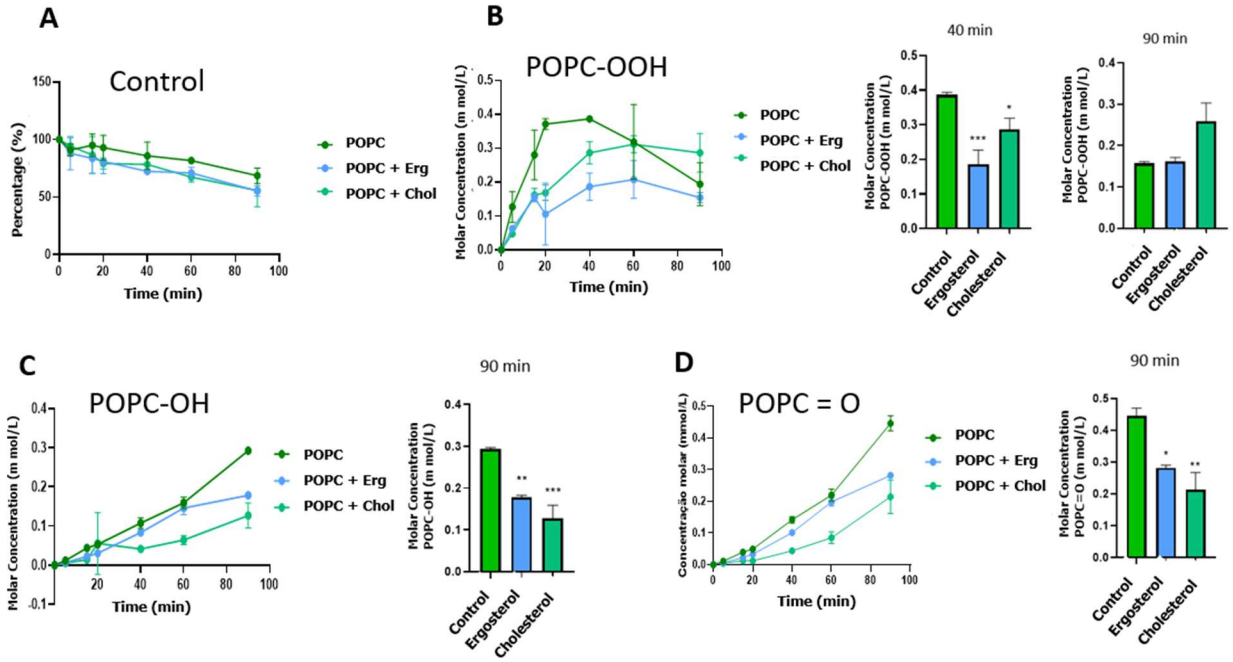

Figure 7. Time-dependent analysis of POPC consumption and formation of photo-oxidation products in liposomes containing only POPC (4 mM), and POPC (1 mM) with cholesterol (Chol) or ergosterol (Erg) (3 mM). (A) Percentage of POPC over the different reaction times with control. Generation of POPC oxidized products: (B) hydroperoxide (POPC-OOH), (C) hydroxide (POPC-OH) and (D) ketone (POPC=O)

426 *Oxidation product consumption kinetics differ among sterols*

427 To determine whether the membrane protective effects of sterols are due to their
428 action as antioxidants or their membrane stabilization effects, we quantified the
429 consumption of sterols and the formation of oxidized products. Notably, Erg was almost
430 totally consumed within the first five minutes of the photooxidation reaction. This
431 consumption was paralleled by the formation of EEP and EHP, with EEP as predominant
432 product. (**Figure 8A**). This indicates that Erg acts as a sacrificial antioxidant protecting
433 membranes from photodamage. Additionally, this data confirms that EEP is the most
434 stable Erg photooxidation product.

435 In contrast to Erg, the consumption and formation of cholesterol oxidation products
436 showed a different profile. While Erg was consumed within the first few minutes,
437 cholesterol consumption and product formation began only after 20 minutes of reaction.
438 Significant formation of cholesterol hydroperoxides (ChOOH) occurred only after 60
439 minutes, showing that cholesterol is not rapidly consumed in the reaction (**Figure 8B**).
440 These data suggest that cholesterol protects membranes against photooxidation primarily
441 through its membrane-stabilizing effects, which shield phospholipid acyl chains from
442 singlet oxygen-mediated oxidation.

443

444

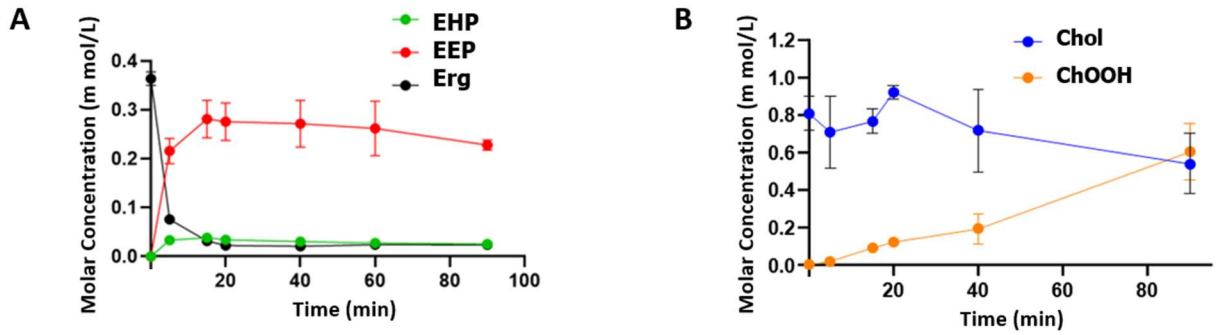

445

446

447 **Figure 8.** Consumption of sterols and oxidation products formed in the reaction with
448 POPC liposomes in the presence of DMMB. Values obtained by peak integration of the
449 detected products in UPLC-MS using the PeakView program. (A) Erg: ergosterol; EHP:
450 ergosterol hydroperoxide; EEP: ergosterol endoperoxide. (B) Chol: cholesterol; ChOOH:

451 cholesterol hydroperoxides

452

453

454 **Photo-oxidized products of sterols show superior A375 cell viability reduction than**
455 **their precursor molecules**

456

457 Considering the EEP the most representative endoperoxide generated by $^1O_2$
458 (type II reaction) as shown previously, we compared the effect of this oxidation product
459 with its precursors: in short, we compared the cell viability of Erg and 7-DHC, with their
460 respective endoperoxides, EEP and CEP. We carried out the assay in four different
461 conditions: (A) PDT, with DMMB and irradiation; (B) with DMMB and without irradiation
462 to evaluate the dark toxicity of DMMB; (C) without DMMB and with irradiation, to evaluate
463 the effect of irradiation; and (D) without DMMB nor irradiation, as a control.

464 **Figure 9** shows the significant reduction in cell viability of A375 cells treated with
465 both endoperoxides, EEP and CEP, in comparison to their precursor molecules, Erg
466 and 7-DHC, respectively. We did not observe significant efficacy of dark toxicity (**Figure**
467 **9B**) or irradiation alone (**Figure 9C**). This experiment evidenced the higher toxicity of
468 endoperoxides, compared to their non-oxidized precursors.

469

470

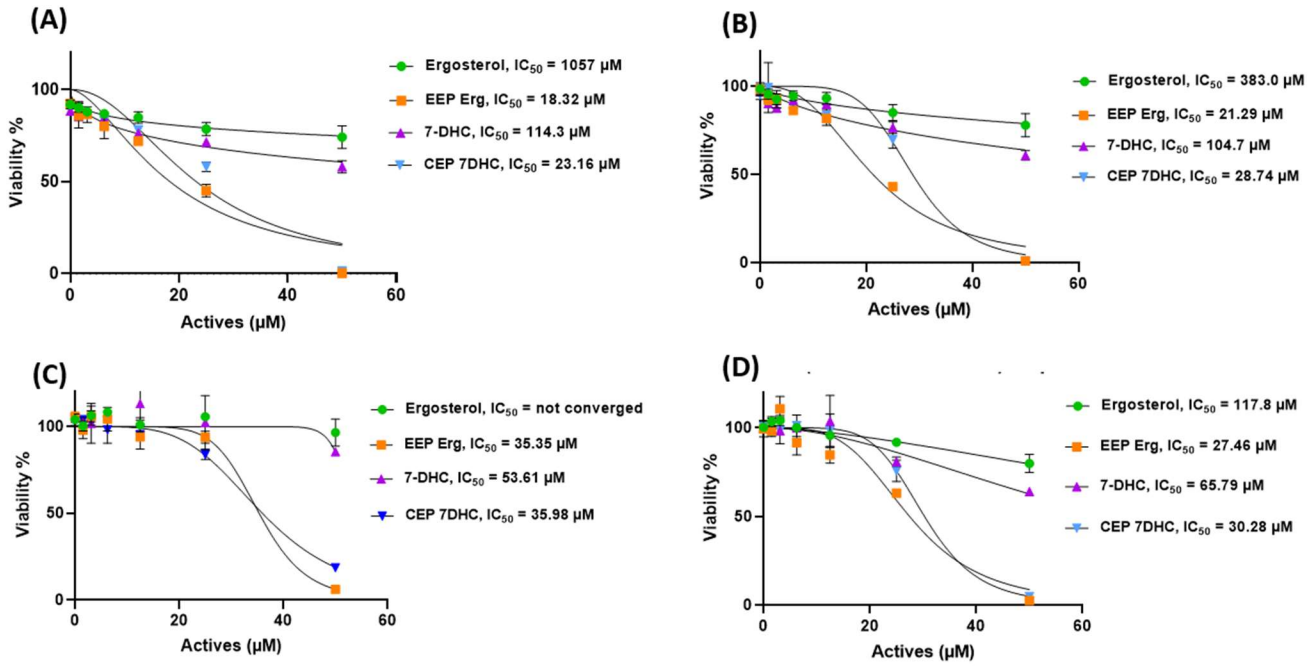

Figure 9. Cell viability effect in A375 with different sterols, ergosterol, ergosterol endoperoxide (EEP Erg), 7-DHC and 7-DHC endoperoxide (CEP): (A) PDT, with DMMB (0.1 nM) and irradiation (5 J/cm^2); (B) with DMMB (0.1 nM) and without irradiation to evaluate the dark toxicity of DMMB; (C) without DMMB and with irradiation (5 J/cm^2); to evaluate the effect of irradiation; and (D) without DMMB and irradiation, as a control

DISCUSSION

Oxidation products of ergosterol by singlet oxygen reaction

Our protocol of type II reaction ($^1O_2$) by DMMB was different compared to other studies. For instance, Böcking *et al*. (2000) (28) used toluene blue as a photosensitizer to generate $^1O_2$ in *S. cerevisiae* and this resulted in the yield of 4.0% DHE followed by 1.5% EEP. Ponce *et al.* (2002) (29) carried out several reactions with rose Bengal and eosin with three types of solvents (pyridine, ethanol, and MTBE), and EEP was the only product generated in all combinations. In their work, Erg + MTBE + eosin generated 16% EEP and, 8% EHP, with trace amounts (not quantifiable) DHE. According to the characterization data of our oxidation product by NMR and mass spectrometry, we

490 confirm that the products synthesized and purified in our work were the same as those
491 found in the literature. This indicates that the main photooxidation products are the same
492 regardless of solvent or photosensitizer type. As mentioned in both our results and in the
493 literature, EEP was the most abundant product in type II Erg oxidation reaction (28–30).
494 Thus, this molecule is a good marker for singlet oxygen reaction, since it is also a stable
495 product at high temperatures (28, 31).
496

497 **Membrane leakage study with carboxyfluorescein using DMMB as a**
498 **photosensitizing agent**

499 In this experiment, the purpose was to investigate membrane leakage caused by
500 the photo-oxidation type II reaction ($^1O_2$) on phospholipid and sterol. Cholesterol-
501 containing liposomes (POPC + Chol) showed lower membrane leakage over time
502 compared to control, Erg- (POPC + Erg) or 7-DHC-liposomes (POPC + Chol) (**Figure**
503 **6A**). This result confirmed the different protection efficacy promoted by sterols,
504 corroborating with data of Tsubone *et al.* (2019) and Bacellar *et al.* (2014) (32, 33), which
505 showed that a liposome formed by DOPC with 30% cholesterol decreased permeability
506 by up to 60% under photo-oxidative stress. Additionally, a study on molecular dynamics
507 by Zhang *et al.* (2018) (34) reported the absence of pore formation in cholesterol-rich
508 membranes, since cholesterol possibly formed hydrogen bonds with the oxidized lipids,
509 making it difficult to generate an inclination in the interaction angles of the lipids. We can
510 also observe the better membrane protection of POPC + Erg and POPC + 7-DHC, but
511 less than the POPC + Chol. This is possibly due to the rapid oxidation of Erg and 7-DHC
512 by type II reaction, leading to an inferior membrane stabilization compared to cholesterol.
513 After some time of reaction, however, all liposomes began to release their internal
514 contents into the external environment. This leakage is possibly due to the formation of
515 truncated phospholipid species bearing aldehyde and carboxylic acid groups from
516 phospholipid hydroperoxides (**Figure 7B**). These truncated lipids favor the deformation
517 of the bilayer and the formation of pores, increasing membrane permeabilization, and
518 generating the release of internal content into the external environment (32).
519

520 **Membrane leakage study with carboxyfluorescein using Fe/Asc as oxidizing agent**

521 Fe/Asc was used as a membrane oxidant to verify the protective efficacy promoted
522 by sterols in liposomes against damage induced by free radicals (type I reaction). Asc
523 reduces Fe (III) into Fe (II). The formation of Fe (II) initiates a Fenton-type reaction with
524 peroxides present in liposomes producing alkoxyl radicals (27). Using 10 μM Fe/Asc, Erg,
525 and 7-DHC provided greater membrane protection compared to control and cholesterol-
526 membrane. However, after a certain period, membrane leakage occurred (**Figure 6B**).
527 Thus, Erg and 7-DHC promoted greater protection of the membrane at the initial phase
528 of lipid peroxidation, but at the propagation phase, the difference among sterols is no
529 longer significant.

530 A study carried out by Freitas *et al.* (2024) (22) also noted that 7-DHC protects the
531 membrane, as it reacts to produce two non-enzymatic 7-DHC oxidation products. This
532 indicates the preference for 7-DHC to be oxidized in place of phospholipids, preventing
533 the formation of truncated species. Although an in-depth study for Erg has not yet been
534 published, the similarity of this molecule to 7-DHC (the presence of the conjugated
535 double-bound present in the sterol B-ring) suggests that Erg may have the same
536 membrane protection function as 7-DHC. Indeed, these authors validated this hypothesis
537 in this same work, in yeast strains with targeted deficiencies of genes important for Erg
538 biosynthesis.

539

540

541 **Oxidation products of liposomes generated by DMMB photooxidation**

542 Our results showed that the generation of phospholipid hydroperoxides (POPC-
543 OOH) was higher in control (POPC) than in membranes containing Erg (POPC + Erg) or
544 cholesterol (POPC + Chol) (**Figure 7B**). However, it is known that the formation of
545 hydroperoxides, hydroxides, and ketones in the acyl chain of the fatty acid esterified to
546 phospholipids does not cause membrane disruption. These products only modify the
547 interactions between phospholipids, leaving the membrane larger and thinner. Instead of
548 them, Bacellar *et al.* (2019) demonstrated that the products responsible for disrupting the
549 membrane are those derived from truncated phospholipids such as POPC aldehyde

550 (AldoPC) or POPC carboxylic acid (PAze PC). These molecules have a different
551 conformation as compared to phospholipids with two chains. In truncated phospholipids,
552 one chain is shorter, presenting a more conical conformation, which may lead to
553 membrane leakage and release of the internal content to the external media (35).

554 Here, formation of AldoPC was not apparent in these liposomes analyzed by
555 UPLC-MS analysis. However, in control sample (POPC) it was possible to detect the
556 maximum formation of POPC-OOH between 20 and 40 minutes, with a subsequent
557 decline, indicating that POPC-OOH started to be consumed after this reaction time
558 (**Figure 7B**). The consumption of hydroperoxides in oxidation reactions is an indication
559 of radical reactions (type I oxidation), caused by the photosensitizer, which can generate
560 truncated lipids such as AldoPC and PAze PC (28). Although liposome with cholesterol
561 (POPC + Chol) formed more POPC-OOH than liposome with ergosterol (POPC + Erg)
562 (**Figure 7B**), there was no indication of consumption of this POPC-OOH in POPC + Chol
563 over the time (**Figure 8B**). This data differs from POPC + Erg, which showed a slight drop
564 in the amount of POPC-OOH after 60 minutes of reaction (**Figure 7B**), supporting a
565 potential initialization of truncated lipids formation. Thus, this difference in the generation
566 of oxidation products, such as hydroperoxides, truncated lipids, and their consumption,
567 illustrates the possible mechanism of faster membrane disruption of Erg-containing
568 liposomes than the cholesterol ones in type II reaction (**Figure 6A**).

569 Tsubone *et al.* (2019) suggested that cholesterol protection is related to the
570 formation of hydrogen bonds with oxidized lipids, making it difficult to change the angle
571 of inclination of the lipids that are interacting, thus maintaining the integrity of the
572 membrane (32). Other work mentioned that cholesterol can reduce the oxygen
573 permeability in the membrane, since there is a greater electron density on both sides of
574 the membrane bilayer when the amount of cholesterol is increased, making the packing
575 of cholesterol with the phospholipid greater, generating a physical barrier to the diffusion
576 of oxygen (36, 37). Our data showed slower consumption of cholesterol and formation of
577 oxidation product (ChOOH) in cholesterol-liposome (**Figures 8A**) than ergosterol in Erg-
578 liposome (**Figures 8B)**. Interestingly, even with distinct oxidation reactions and liposomes
579 composition, such as 1,2-dipalmitoyl-sn-glycero-3-phosphocholine (DPPC) and 1-
580 palmitoyl-2-oleoyl-sn-glycero-3 -phospho-(1'-rac- glycerol) (POPG) in different works (32,

581 34), they showed the same tendency which confirms the consistency of our results.
582 As a complement, an interesting work using plant extract also evidenced the
583 antioxidant and physical adsorption mechanisms of several plants to protect membrane,
584 measured via CF emission in DMMB-liposomes. Gallic acid and trehalose were used as
585 standard compounds, and the percentage of membrane protection was linearly
586 proportional to the concentration of these compounds, highlighting the several
587 mechanisms of compounds influencing the membrane integrity (38).
588

589 **Cell viability effect of sterols and photodynamic therapy in the melanoma A375 cell**
590 **line**

591 Our results showed significant reduction in cell viability of melanoma A375 cells
592 treated with sterol endoperoxides. EEP and CEP, the endoperoxides of Erg and 7-DHC,
593 respectively, showed greater efficacy in killing melanoma cells compared to their
594 precursors. Higher cytotoxicity of sterol endoperoxides was also reported in other cancer
595 cells. On A549 lung cancer cells, authors showed greater cell viability inhibition of EEP to
596 Erg and 9,11-dehydroergosterol endoperoxide. According to their work, EEP induced
597 caspase-dependent apoptosis via mitochondrial damage, cytochrome c release, and
598 ROS generation (39). Furthermore, the superior cytotoxicity of endoperoxides derived
599 from ergosterol and 7-DHC has been also evidenced in lung cancer A547, cervical
600 carcinoma cells HeLa, breast cancer cells SKOV-3, prostatic carcinoma cells DU145, and
601 human normal liver cells L-02 (40).
602 Other interesting work with 7-DHC demonstrated the influence of this sterol on
603 ferroptosis, an iron-dependent and non-apoptotic cell death induced by accumulation of
604 membrane-destabilizing truncated phospholipid species. These authors identified 7-DHC
605 as a suppressor of ferroptosis, due to its high reactivity towards peroxyl radicals, which
606 protects polyunsaturated fatty acids (PUFAs) from peroxidation. Although the unsaturated
607 B rings in 7-DHC make it a primary target for peroxidation, acting as a sacrificial
608 antioxidant, the oxidized 7-DHC metabolites have a lower membrane-destabilizing effect
609 compared to truncated species. This may provide a membrane-shielding effect that
610 reduces cell death. Membrane leakage tests showed superior membrane protection of 7-

611 DHC compared to control and cholesterol against radicals produced by the Fe/Asc
612 system (22). This result is in line with our results of 7-DHC-membrane leakage using
613 Fe/Asc (type I reaction) and carboxyfluorescein.

614 Another work detected the location of 7-DHC inside the cells, which was both in
615 the mitochondria and the plasma membrane. Authors demonstrated the 7-DHC as
616 suppressor of phospholipid peroxidation to reduce ferroptosis in both locations. They
617 showed that Erg, the analogue of 7-DHC, also suppressed ferroptosis. By adding RSL3
618 (ferroptosis-inducing agent) to HEK293T cells pre-treated with 7-DHC, Erg, stigmasterol,
619 or cholesterol, they showed that Erg and 7-DHC blocked phospholipid autooxidation and
620 inhibited ferroptosis, unlike other sterols (21).

621 As the mechanism of ferroptosis relies on the high susceptibility of PUFAs in
622 phospholipid membranes to lipid peroxidation, it leads to the accumulation of lipid
623 peroxides and cell death. Nevertheless, it is known that lipid droplets (LDs), the lipid-rich
624 cellular organelles, incorporate excess PUFAs within their neutral core, controlling PUFA
625 storage in the form of triacylglycerols and sterol esters to reduce potential lipotoxic
626 damage (41). It was shown that the formation of LDs induced by cell cycle arrest promoted
627 resistance to ferroptosis. Authors showed that diacylglycerol acyltransferase (DGAT)-
628 dependent LDs were formed under induction by cell cycle arrest. This LD sequestered
629 excessive PUFAs accumulated in cells to suppress ferroptosis, and the inhibition of DGAT
630 resensitized the cell arrest to ferroptosis (42). Moreover, as LDs disruption can provide
631 the release of excessive lipids to generate increased lipid peroxidation, LDs can act in
632 both prevention or induction of lipotoxicity and cell death, depending on the oxidative
633 stress. Additional information is provided by other authors, indicating that the $^1O_2$
634 generated by PDT can induce both apoptosis and ferroptosis, according to the $^1O_2$ dose.
635 They described that a moderate dose of singlet oxygen induces apoptosis, releasing cyt
636 c from mitochondria. However, an excessive dose of $^1O_2$ inactivates cyt c and caspase
637 enzymes, inhibiting this pathway and inducing ferroptosis by excess lipid peroxidation
638 combined with iron release from lysosomal membrane disruption (43).

639 Interestingly, it is reported that Erg can also be stored in LD as sterol ester, and
640 this would prevent lipid peroxidation that leads to ferroptosis (44). A study demonstrated
641 that the mitochondrial concentration of Erg in *S. cerevisiae* was mainly located in the inner

642 mitochondrial membrane (IMM) than in the outer mitochondrial membrane (OMM), and
643 this sterol is actively transported into the OMM in an energy-independent way. Since
644 mitochondria communicate with LDs, endoplasmic reticulum (ER), and peroxisomes (45),
645 the Erg LD storage might be influenced by the correct function of mitochondria. In
646 contrast, a work evidenced that the endoperoxide EEP inhibited LD synthesis of
647 differentiated 3T3-L1 cells (46), indicating the opposite effects of Erg and EEP on LD
648 formation.

649 Concerning the role of mitochondria, it is well known that this organelle and
650 lysosome are the main target organelles for type II reaction ($^1O_2$) by PDT (35). Although
651 lipid peroxidation in the endoplasmic reticulum and plasma membrane highly influences
652 ferroptosis, mitochondria have also a contribution to this cell death process (47). It is
653 described that PDT with DMMB reduced mitochondrial membrane potential and promoted
654 increased reactive oxygen species production, autophagic dysfunction, and increased
655 membrane permeability. DMMB easily diffuses through the plasma membrane and, due
656 to its positive charge, accumulates in the mitochondria, an organelle with an inner
657 negative charge (48). It is reported that PDT with DMMB promoted loss of membrane
658 potential of mitochondria in the parasite *Leishmania amazonensis*, and released lipids
659 into the cytosol. Additionally, LDs increased substantially and accumulated large amounts
660 of these free lipids. This response of LDs to mitochondrial dysfunction regulates
661 lipotoxicity and preserves organelle function to prevent cell death. However, a redox
662 imbalance caused by lipid overload possibly led to constant cellular stress, and the
663 parasite's final death (49).

664 As a complement, a clinical test with PDT by intratumorally injection of 2%
665 methylene blue aqueous solution with 2% lidocaine, in a 92-years-old multiple skin
666 melanoma patient, showed a tumor remission in five out of six sites of tumors, highlighting
667 the potential of PDT as an effective and inexpensive treatment for melanoma (50).

668

669 All above studies could provide several insights into the cell death mechanism in
670 A375 cells in this work, as follows:

671 First, the membrane permeability property changes according to the type of
672 oxidative damage. In the type I reaction, superior membrane protection against leakage

673 was observed in Erg and 7-DHC than control and cholesterol in the initiation phase of
674 lipid peroxidation. This agrees with the results presented by Freitas *et al.* (2024) (22),
675 indicating the effectiveness of 5,7-unsaturated sterols against type I reaction in the initial
676 phase of lipid peroxidation. This is possibly due to the radical trapping ability (51) and
677 reduced formation of truncated lipids in the membranes when these sterols are introduced
678 (22). This result, however, differs from type II oxidation, where cholesterol protected the
679 membrane more than Erg and 7-DHC. This fact can be explained by the results shown
680 in **Figures 8A** and **8B** of our work, where there is a significant difference in sterol
681 consumption. Erg is almost immediately consumed and generates EEP or EHP, while
682 cholesterol consumption and generation of its main hydroperoxide (ChOOH) takes much
683 longer under type II photo-oxidation. As cited previously, cholesterol-rich membranes
684 reported the absence of pore formation possibly due to the hydrogen bonds formation
685 with the oxidized lipids (34).

686 Second, the protection of cells against ferroptosis in Li *et al.* (2024) and Freitas *et*
687 *al.* (2024) (21, 22) had a greater effect with 7-DHC than the controls. Our results also
688 showed a non-significant cell viability reduction in A375 cells treated with 7-DHC and Erg.
689 Here we can raise some hypotheses. The non-excessive dose of $^1O_2$ by PDT (type II
690 reaction) in our work led to the formation of a small amount of their respective
691 endoperoxides, not enough to kill the cells, but enough to protect the membranes from
692 truncated lipid formation. Another hypothesis might be the high amount of both sterols
693 that induced the formation of LDs, avoiding lipotoxicity and cell death, but still to be
694 confirmed.

695 Third, EEP and CEP promoted opposite effects to their precursor molecules, Erg
696 and 7-DHC. These endoperoxides led to cell death, while Erg and 7-DHC did not.
697 According to the work by Wu *et al.* (2018) (39) mentioned previously, EEP induces
698 caspase-dependent apoptosis via mitochondrial damage, cytochrome c release, and
699 ROS generation, and induces mitophagy at 20 μM. Interestingly, our work showed a
700 sudden decline of cell viability mostly after 20 μM EEP (**Figure 9**), which highlights the
701 need for additional studies to deepen this dose-dependent mechanism. Our results
702 may also be in line with the description of Fujii *et al.* (2023) (43), which suggests that
703 a moderate dose of $^1O_2$ mainly induces apoptosis rather than ferroptosis. An additional

704 explanation for the reduction of cell viability may be the lipotoxicity due to the excess
705 concentration of EEP. EEP suppressed the lipid droplet synthesis by inhibiting
706 triglyceride synthesis in differentiated 3T3-L1 cells (46). Another study with 24(S)-
707 hydroxycholesterol showed that its esterification resulted in the formation of atypical
708 lipid droplets due to the endoplasmic reticulum membrane disorder. This was caused
709 by the change of polarity of this sterol by esterification, disturbing membrane bilayer
710 orientation (52). Although they differ in structure, changes in molecular polarity
711 induced by enzymatic or non-enzymatic processes may lead to non-controlled
712 lipotoxicity and increased cell death. This information may inspire future investigations
713 concerning the influence of oxidation products on the rupture of LDs, to promote
714 lipotoxicity (49). Another explanation could be the generation of a second metabolite
715 of EEP and CEP under PDT. However, as shown in **Figure S6**, EEP is highly stable,
716 suggesting that the effect of PDT on the already-formed EEP may not be highly
717 significant. All these descriptions strongly highlight that these endoperoxides have
718 different efficacy compared to their precursor molecules, and dose and stress
719 conditions may be one of the key triggers to direct cell death pathways.
720 Although additional studies are still expected to confirm these explanations, the
721 originality of this work relies on the description of the step-by-step process to generate
722 and identify endoperoxide through the type II reaction, and it also provides new insights
723 to elucidate different mechanisms of cell death promoted by Erg, 7-DHC and their
724 respective endoperoxides, in combination with PDT in A375 melanoma cells.
725

726 **CONCLUSION**

727

728 Melanoma is one of the most aggressive oncological diseases that require effective
729 treatment. Ergosterol is a sterol from a natural source that has attracted attention for its
730 several benefits. 7-DHC, an analog of Erg present in the human membrane, has also
731 shown benefits in several diseases, including cancer. However, some ambiguity or
732 uncertainty remains regarding the mechanism of their protective or deleterious effects.
733 Focusing on the mechanistic point of view of the cell membrane lipid bilayer, we used the
734 liposome leakage model to compare the possible causes of membrane rupture in distinct

types of lipid oxidation reactions. We then evaluated the cell viability of A375 melanoma treated with 7-DHC and Erg, and their respective endoperoxides generated by the type II oxidative reaction.

The protocol carried out in this work confirmed the generation of Erg endoperoxide and other sterols. The membrane leakage results demonstrated different behaviors between liposomes composed of Erg, 7-DHC or cholesterol under distinct oxidation reactions (type I and II). When correlating our results with the literature, the presence of truncated lipids generated by oxidative stress appears to be the main cause of membrane integrity disruption, compromising cell viability. In vitro viability testing of A375 melanoma cells with PDT showed inhibition of cell viability in endoperoxide-treated cells and no significant reduction in precursor molecules. These results in combination with data from the literature pointed out some directions, such as the influence of these sterols and derivatives combined with singlet oxygen on apoptosis, ferroptosis, mitochondria integrity and formation of lipid droplets. The change in increased or decreased cell viability appears to be highly dependent on the dose of oxidative stress and the concentration or type of sterols.

Thus, in this work, unlike other studies, we explored the possible effects of Erg and 7-DHC oxidation derivatives generated mainly by the type II reaction and highlighted the different effects of sterols and their endoperoxide derivatives on the cell viability of the A375 melanoma cell line.

ACKNOWLEDGMENTS:

This study was supported by Fundação de Amparo à Pesquisa do Estado de São Paulo [FAPESP, CEPID–Redoxoma grant 13/07937-8 to S.M., and M.S.B, and P.D.M.], [FAPESP, nbr. 2023/15361-0 to M.N.Y.], [FAPESP, 23/12767-6 to T.E.O.S.], Conselho Nacional de Desenvolvimento Científico e Tecnológico [CNPq 313926/2021-2 to S.M.], [CNPq nº. 304350/2023-0 to P.D.M.], Coordenação de Aperfeiçoamento de Pessoal de Nível Superior [CAPES, Finance Code 001] , Pro-Reitoria de Pesquisa da Universidade de São Paulo [PRPUSP], NAP Redoxoma [nº. 2011.1.9352.1.8 tp P.D.M] and the John Simon Guggenheim Memorial Foundation to P.D.M.

765

766 **CONFLICT OF INTEREST**

767 The authors declare that they have no known competing financial interests or
768 personal relationships that could have appeared to influence the work reported in this
769 paper.

770

771 **SUPPLEMENTARY MATERIALS**

772 See supplementary materials.

773

774 **REFERENCES**

775 1. Zeng, L., Gowda, B. H. J., Ahmed, M. G., Abourehab, M. A. S., Chen, Z. S., Zhang, C.,
776 Li, J. and Kesharwani, P. (2023) Advancements in nanoparticle-based treatment
777 approaches for skin cancer therapy. *Mol Cancer* **22**. https://doi.org/10.1186/s12943-022-
778 01708-4.

779 2. Arnold, M., Singh, D., Laversanne, M., Vignat, J., Vaccarella, S., Meheus, F., Cust, A.
780 E., De Vries, E., Whiteman, D. C. and Bray, F. (2022) Global Burden of Cutaneous
781 Melanoma in 2020 and Projections to 2040. *JAMA Dermatol* **158**, 495–503.
782 https://doi.org/10.1001/jamadermatol.2022.0160.

783 3. Erem, A. S. and Razzaque, M. S. (2021) Vitamin D-independent benefits of safe
784 sunlight exposure. *Journal of Steroid Biochemistry and Molecular Biology* **213**.
785 https://doi.org/10.1016/j.jsbmb.2021.105957.

786 4. Bastos, E. L., Quina, F. H. and Baptista, M. S. (2022) Endogenous Photosensitizers in
787 Human Skin. *Chem Rev*. https://doi.org/10.1021/acs.chemrev.2c00787.

788 5. Tonolli, P. N., Vera Palomino, C. M., Junqueira, H. C. and Baptista, M. S. (2023) The
789 phototoxicity action spectra of visible light in HaCaT keratinocytes. *J Photochem*
790 *Photobiol B* **243**. https://doi.org/10.1016/j.jphotobiol.2023.112703.

791 6. Di Mascio, P., Martinez, G. R., Miyamoto, S., Ronsein, G. E., Medeiros, M. H. G. and
792 Cadet, J. (2019) Singlet Molecular Oxygen Reactions with Nucleic Acids, Lipids, and
793 Proteins. *Chem Rev* **119**, 2043–2086. https://doi.org/10.1021/acs.chemrev.8b00554.

794 7. Cadet, J., Angelov, D., Di Mascio, P. and Wagner, J. R. (2024) Contribution of oxidation
795 reactions to photo-induced damage to cellular DNA. *Photochem Photobiol*.
796 https://doi.org/10.1111/php.13990.
797 8. Harayama, T. and Riezman, H. (2018) Understanding the diversity of membrane lipid
798 composition. *Nat Rev Mol Cell Biol* **19**, 281–296. https://doi.org/10.1038/nrm.2017.138.
799 9. Ikonen, E. (2008) Cellular cholesterol trafficking and compartmentalization. *Nat Rev*
800 *Mol Cell Biol* **2**, 125–138. https://doi.org/10.1038/nrm2336.
801 10. Payne, A. H. and Hales, D. B. (2004) Overview of steroidogenic enzymes in the
802 pathway from cholesterol to active steroid hormones. *Endocr Rev* **25**, 947–970.
803 https://doi.org/10.1210/er.2003-0030.
804 11. Miyamoto, S., Lima, R. S., Inague, A. and Viviani, L. G. (2021) Electrophilic oxysterols:
805 generation, measurement and protein modification. *Free Radic Res* **55**, 416–440.
806 https://doi.org/10.1080/10715762.2021.1879387.
807 12. Ellis, M. T. (1918) Contributions to our Knowledge of the Plant Sterols. Part II. _1918.
808 *Biochemical Journal* **12**, 173–177. https://doi.org/10.1042/bj0120173.
809 13. Weete, J. D., Abril, M. and Blackwell, M. (2010) Phylogenetic distribution of fungal
810 sterols. *PLoS One* **5**. https://doi.org/10.1371/journal.pone.0010899.
811 14. Shimizu, T., Kawai, J., Ouchi, K., Kikuchi, H., Osima, Y. and Hidemi, R. (2016) Agarol,
812 an ergosterol derivative from Agaricus blazei, induces caspase-independent apoptosis in
813 human cancer cells. *Int J Oncol* **48**, 1670–1678. https://doi.org/10.3892/ijo.2016.3391.
814 15. Rhee, Y. H., Jeong, S. J., Lee, H. J., Lee, H. J., Koh, W., Jung, J. H., Kim, S. H. and
815 Sung-Hoon, K. (2012) Inhibition of STAT3 signaling and induction of SHP1 mediate
816 antiangiogenic and antitumor activities of ergosterol peroxide in U266 multiple myeloma
817 cells. *BMC Cancer* **12**. https://doi.org/10.1186/1471-2407-12-28.
818 16. Li, X., Wu, Q., Bu, M., Hu, L., Du, W. W., Jiao, C., Pan, H., Sdiri, M., Wu, N., Xie, Y.
819 and Yang, B. B. (2016) Ergosterol peroxide activates Foxo3-mediated cell death
820 signaling...hepatocellular carcinoma cells_2016. *Oncotarget* **7**, 33948–33959.
821 https://doi.org/10.18632/oncotarget.8608.
822 17. Sokolov, S. S., Akimov, S. A. and Severin, F. F. (2024) Evolutionary Choice between
823 Cholesterol and Ergosterol. *Biochem (Mosc) Suppl Ser A Membr Cell Biol* **18**, 219–223.
824 https://doi.org/10.1134/S1990747824700211.

825 18. Kuwabara, N., Ohta-Shimizu, M., Fuwa, F., Tomitsuka, E., Sato, S. and Nakagawa,
826 S. (2022) Ergosterol increases 7-dehydrocholesterol, a cholesterol precursor, and
827 decreases cholesterol in human HepG2 cells. *Lipids* **57**, 303–311.
828 https://doi.org/10.1002/lipd.12357.
829 19. Gelzo, M., Granato, G., Albano, F., Arcucci, A., Dello Russo, A., De Vendittis, E.,
830 Ruocco, M. R. and Corso, G. (2014) Evaluation of cytotoxic effects of 7-
831 dehydrocholesterol on melanoma cells. *Free Radic Biol Med* **70**, 129–140.
832 https://doi.org/10.1016/j.freeradbiomed.2014.02.013.
833 20. Wang, Y., Tian, N., Li, C., Hou, Y., Wang, X. and Zhou, Q. (2019) Incorporation of 7-
834 dehydrocholesterol into liposomes as a simple, universal and efficient way to enhance
835 anticancer activity by combining PDT and photoactivated chemotherapy. *Chemical*
836 *Communications* **55**, 14081–14084. https://doi.org/10.1039/c9cc05691b.
837 21. Li, Y., Ran, Q., Duan, Q., Jin, J., Wang, Y., Yu, L., Wang, C., Zhu, Z., Chen, X., Weng,
838 L., Li, Z., Wang, J., Wu, Q., Wang, H., Tian, H., Song, S., Shan, Z., Zhai, Q., Qin, H.,
839 Chen, S., Fang, L., Yin, H., Zhou, H., Jiang, X. and Wang, P. (2024) 7-Dehydrocholesterol
840 dictates ferroptosis sensitivity. *Nature* **626**, 411–418. https://doi.org/10.1038/s41586-023-
841 06983-9.
842 22. Freitas, F. P., Alborzinia, H., dos Santos, A. F., Nepachalovich, P., Pedrera, L., Zilka,
843 O., Inague, A., Klein, C., Aroua, N., Kaushal, K., Kast, B., Lorenz, S. M., Kunz, V.,
844 Nehring, H., Xavier da Silva, T. N., Chen, Z., Atici, S., Doll, S. G., Schaefer, E. L., Ekpo,
845 I., Schmitz, W., Horling, A., Imming, P., Miyamoto, S., Wehman, A. M., Genaro-Mattos,
846 T. C., Mirnics, K., Kumar, L., Klein-Seetharaman, J., Meierjohann, S., Weigand, I., Kroiss,
847 M., Bornkamm, G. W., Gomes, F., Netto, L. E. S., Sathian, M. B., Konrad, D. B., Covey,
848 D. F., Michalke, B., Bommert, K., Bargou, R. C., Garcia-Saez, A., Pratt, D. A., Fedorova,
849 M., Trumpp, A., Conrad, M. and Friedmann Angeli, J. P. (2024) 7-Dehydrocholesterol is
850 an endogenous suppressor of ferroptosis. *Nature* **626**, 401–410.
851 https://doi.org/10.1038/s41586-023-06878-9.
852 23. Miyamoto, S., Nantes, I. L., Faria, P. A., Cunha, D., Ronsein, G. E., Medeiros, M. H.
853 G. and Di Mascio, P. (2012) Cytochrome c-promoted cardiolipin oxidation generates
854 singlet molecular oxygen. *Photochemical and Photobiological Sciences* **11**, 1536–1546.
855 https://doi.org/10.1039/c2pp25119a.

24. Martins, W. K., Santos, N. F., Rocha, C. de S., Bacellar, I. O. L., Tsubone, T. M., Viotto, A. C., Matsukuma, A. Y., Abrantes, A. B. de P., Siani, P., Dias, L. G. and Baptista, M. S. (2019) Parallel damage in mitochondria and lysosomes is an efficient way to photoinduce cell death. *Autophagy* **15**, 259–279. https://doi.org/10.1080/15548627.2018.1515609.

25. Freitas, J. V., Junqueira, H. C., Martins, W. K., Baptista, M. S. and Gaspar, L. R. (2019) Antioxidant role on the protection of melanocytes against visible light-induced photodamage. *Free Radic Biol Med* **131**, 399–407. https://doi.org/10.1016/j.freeradbiomed.2018.12.028.

26. Lang, J. K. and Vigo-Pelfrey, C. (1993) Quality control of liposomal lipids with special emphasis on peroxidation of phospholipids and cholesterol.

27. Saito, R. F., Rangel, M. C., Halman, J. R., Chandler, M., de Sousa Andrade, L. N., Odete-Bustos, S., Furuya, T. K., Carrasco, A. G. M., Chaves-Filho, A. B., Yoshinaga, M. Y., Miyamoto, S., Afonin, K. A. and Chammas, R. (2021) Simultaneous silencing of lysophosphatidylcholine acyltransferases 1-4 by nucleic acid nanoparticles (NANPs) improves radiation response of melanoma cells. *Nanomedicine* **36**. https://doi.org/10.1016/j.nano.2021.102418.

28. Böcking, T., Barrow, K. D., Netting, A. G., Chilcott, T. C., Coster, H. G. L. and Höfer, M. (2000) Effects of singlet oxygen on membrane sterols in the yeast Saccharomyces cerevisiae. *Eur J Biochem* **267**, 1607–1618. https://doi.org/10.1046/j.1432-1327.2000.01179.x.

29. Ponce, M. A., Ramirez, J. A., Galagovsky, L. R., Gros, E. G. and Erra-Balsells, R. (2002) A new look into the reaction between ergosterol and singlet oxygen in vitro. *Photochemical and Photobiological Sciences* **1**, 749–756. https://doi.org/10.1039/b204452h.

30. Khan, Z. U., Khan, L. U., Uchiyama, M. K., Prado, F. M., Faria, R. L., Costa, I. F., Miyamoto, S., Araki, K., Gidlund, M., Brito, H. F. and Di Mascio, P. (2023) Singlet Molecular Oxygen Generation via Unexpected Emission Color-Tunable CdSe/ZnS Nanocrystals for Applications in Photodynamic Therapy. *ACS Appl Nano Mater* **6**, 3767–3780. https://doi.org/10.1021/acsanm.2c05482.

31. Ling, T., Lang, W. H., Martinez-Montemayor, M. M. and Rivas, F. (2019) Development

887 of ergosterol peroxide probes for cellular localisation studies. *Org Biomol Chem* **17**, 5223–
888 5229. https://doi.org/10.1039/c9ob00145j.
889 32. Tsubone, T. M., Baptista, M. S. and Itri, R. (2019) Understanding membrane
890 remodelling initiated by photosensitized lipid oxidation. *Biophys Chem* **254**.
891 https://doi.org/10.1016/j.bpc.2019.106263.
892 33. Bacellar, I. O. L., Pavani, C., Sales, E. M., Itri, R., Wainwright, M. and Baptista, M. S.
893 (2014) Membrane damage efficiency of phenothiazinium photosensitizers. *Photochem*
894 *Photobiol* **90**, 801–813. https://doi.org/10.1111/php.12264.
895 34. Zhang, X., Barraza, K. M. and Beauchamp, J. L. (2018) Cholesterol provides
896 nonsacrificial protection of membrane lipids from chemical damage at air–water interface.
897 *Proc Natl Acad Sci U S A* **115**, 3255–3260. https://doi.org/10.1073/pnas.1722323115.
898 35. Bacellar, I. O. L. and Baptista, M. S. (2019) Mechanisms of Photosensitized Lipid
899 Oxidation and Membrane Permeabilization. *ACS Omega* **4**, 21636–21646.
900 https://doi.org/10.1021/acsomega.9b03244.
901 36. Dotson, R. J., Smith, C. R., Bueche, K., Angles, G. and Pias, S. C. (2017) Influence
902 of Cholesterol on the Oxygen Permeability of Membranes: Insight from Atomistic
903 Simulations. *Biophys J* **112**, 2336–2347. https://doi.org/10.1016/j.bpj.2017.04.046.
904 37. Bacellar, I. O. L., Cordeiro, R. M., Mahling, P., Baptista, M. S., Röder, B. and
905 Hackbarth, S. (2019) Oxygen distribution in the fluid/gel phases of lipid membranes.
906 *Biochim Biophys Acta Biomembr* **1861**, 879–886.
907 https://doi.org/10.1016/j.bbamem.2019.01.019.
908 38. Silva, D. R., Cabello, M. C., Severino, D. and Baptista, M. S. (2021) Performance of
909 Cosmetic Ingredients Evaluated by Their Membrane Protection Efficiency. *Journal of*
910 *Cosmetics, Dermatological Sciences and Applications* **11**, 169–185.
911 https://doi.org/10.4236/jcdsa.2021.113016.
912 39. Wu, H. Y., Yang, F. L., Li, L. H., Rao, Y. K., Ju, T. C., Wong, W. T., Hsieh, C. Y.,
913 Pivkin, M. V., Hua, K. F. and Wu, S. H. (2018) Ergosterol peroxide from marine fungus
914 Phoma sp. induces ROS-dependent apoptosis and autophagy in human lung
915 adenocarcinoma cells. *Sci Rep* **8**. https://doi.org/10.1038/s41598-018-36411-2.
916 40. Tian, N. N., Li, C., Tian, N., Zhou, Q. X., Hou, Y. J., Zhang, B. W. and Wang, X. S.
917 (2017) Syntheses of 7-dehydrocholesterol peroxides and their improved anticancer

918 activity and selectivity over ergosterol peroxide. *New Journal of Chemistry* **41**, 14843–
919 14846. https://doi.org/10.1039/c7nj04100d.
920 41. Danielli, M., Perne, L., Jarc Jovičić, E. and Petan, T. (2023) Lipid droplets and
921 polyunsaturated fatty acid trafficking: Balancing life and death. *Front Cell Dev Biol* **11**.
922 https://doi.org/10.3389/fcell.2023.1104725.
923 42. Lee, H., Horbath, A., Kondiparthi, L., Meena, J. K., Lei, G., Dasgupta, S., Liu, X.,
924 Zhuang, L., Koppula, P., Li, M., Mahmud, I., Wei, B., Lorenzi, P. L., Keyomarsi, K.,
925 Poyurovsky, M. V., Olszewski, K. and Gan, B. (2024) Cell cycle arrest induces lipid droplet
926 formation and confers ferroptosis resistance. *Nat Commun* **15**.
927 https://doi.org/10.1038/s41467-023-44412-7.
928 43. Fujii, J., Soma, Y. and Matsuda, Y. (2023) Biological Action of Singlet Molecular
929 Oxygen from the Standpoint of Cell Signaling, Injury and Death. *Molecules* **28**.
930 https://doi.org/10.3390/molecules28104085.
931 44. Hapala, I., Griac, P. and Holic, R. (2020) Metabolism of Storage Lipids and the Role
932 of Lipid Droplets in the Yeast Schizosaccharomyces pombe. *Lipids* **55**, 513–535.
933 https://doi.org/10.1002/lipd.12275.
934 45. Cirigliano, A., Macone, A., Bianchi, M. M., Oliaro-Bosso, S., Balliano, G., Negri, R.
935 and Rinaldi, T. (2019) Ergosterol reduction impairs mitochondrial DNA maintenance in S.
936 cerevisiae. *Biochim Biophys Acta Mol Cell Biol Lipids* **1864**, 290–303.
937 https://doi.org/10.1016/j.bbalip.2018.12.002.
938 46. Jeong, Y. U. and Park, Y. J. (2020) Ergosterol peroxide from the medicinal mushroom
939 ganoderma lucidum inhibits differentiation and lipid accumulation of 3T3-L1 adipocytes.
940 *Int J Mol Sci* **21**. https://doi.org/10.3390/ijms21020460.
941 47. von Krusenstiern, A. N., Robson, R. N., Qian, N., Qiu, B., Hu, F., Reznik, E., Smith,
942 N., Zandkarimi, F., Estes, V. M., Dupont, M., Hirschhorn, T., Shchepinov, M. S., Min, W.,
943 Woerpel, K. A. and Stockwell, B. R. (2023) Identification of essential sites of lipid
944 peroxidation in ferroptosis. *Nat Chem Biol* **19**, 719–730. https://doi.org/10.1038/s41589-
945 022-01249-3.
946 48. de Ávila Narciso Gomes, R., Marmolejo-Garza, A., Haan, F. J., García, T. M., Chen,
947 T., Mauthe, M., Moreira Franco Parisotto, Y. E., Murakami, M. M., Marie, S. K. N.,
948 Baptista, M. S., Dolga, A. M. and Trombetta-Lima, M. (2023) Mitochondrial dysfunction

949 mediates neuronal cell response to DMMB photodynamic therapy. *Biochim Biophys Acta*
950 *Mol Cell Res* **1870**. https://doi.org/10.1016/j.bbamcr.2022.119429.
951 49. Cabral, F. V., Cerone, M., Persheyev, S., Lian, C., Samuel, I. D. W., Ribeiro, M. S.
952 and Smith, T. K. (2023) New insights in photodynamic inactivation of Leishmania
953 amazonensis: A focus on lipidomics and resistance. *PLoS One* **18**.
954 https://doi.org/10.1371/journal.pone.0289492.
955 50. Tardivo, J. P., Del Giglio, A., Paschoal, L. H. C., Ito, A. S. and Baptista, M. S. (2004)
956 Treatment of melanoma lesions using methylene blue and RL50 light source.
957 *Photodiagnosis Photodyn Ther* **1**, 345–346. https://doi.org/10.1016/S1572-
958 1000(05)00005-0.
959 51. Yamada, N., Karasawa, T., Ito, J., Yamamuro, D., Morimoto, K., Nakamura, T.,
960 Komada, T., Baatarjav, C., Saimoto, Y., Jinnouchi, Y., Watanabe, K., Miura, K., Yahagi,
961 N., Nakagawa, K., Matsumura, T., Yamada, K. I., Ishibashi, S., Sata, N., Conrad, M. and
962 Takahashi, M. (2024) Inhibition of 7-dehydrocholesterol reductase prevents hepatic
963 ferroptosis under an active state of sterol synthesis. *Nat Commun* **15**.
964 https://doi.org/10.1038/s41467-024-46386-6.
965 52. Takabe, W., Urano, Y., Ho Vo, D. K., Shibuya, K., Tanno, M., Kitagishi, H., Fujimoto,
966 T. and Noguchi, N. (2016) Esterification of 24S-OHC induces formation of atypical lipid
967 droplet-like structures, leading to neuronal cell death. *J Lipid Res* **57**, 2005–2014.
968 https://doi.org/10.1194/jlr.M068775.
969